



HAL
open science

Tailoring crystallisation of anatase TiO₂ ultra-thin films grown by atomic layer deposition using 2D oxides as growth template

André Grishin, Bruno Bérini, Maxime Vallet, Simon Hurand, Florian Maudet, Corinne Sartel, Mathieu Frégnaux, Sophie Nowak, Gaëlle Amiri, Said S. Hassani, et al.

► To cite this version:

André Grishin, Bruno Bérini, Maxime Vallet, Simon Hurand, Florian Maudet, et al.. Tailoring crystallisation of anatase TiO₂ ultra-thin films grown by atomic layer deposition using 2D oxides as growth template. *Applied Surface Science*, 2023, 641, pp.158446. 10.1016/j.apsusc.2023.158446 . hal-04229560

HAL Id: hal-04229560

<https://hal.science/hal-04229560>

Submitted on 10 Oct 2023

HAL is a multi-disciplinary open access archive for the deposit and dissemination of scientific research documents, whether they are published or not. The documents may come from teaching and research institutions in France or abroad, or from public or private research centers.

L'archive ouverte pluridisciplinaire **HAL**, est destinée au dépôt et à la diffusion de documents scientifiques de niveau recherche, publiés ou non, émanant des établissements d'enseignement et de recherche français ou étrangers, des laboratoires publics ou privés.

Copyright

Tailoring crystallisation of anatase TiO₂ ultra-thin films grown by Atomic Layer Deposition using 2D oxides as growth template

André Grishin¹, Bruno Bérini^{1,}, Maxime Vallet², Simon Hurand³, Florian Maudet⁴, Corinne Sartel¹, Mathieu Frégnaux⁵, Sophie Nowak⁶, Gaëlle Amiri¹, Said Hassani¹, Damien Aureau⁵, Vincent Sallet¹, Valérie Demange⁷ and Yves Dumont^{1,*}*

¹ Université Paris-Saclay, UVSQ, CNRS, GEMaC UMR8635, 78035, Versailles, France

² Université Paris-Saclay, CentraleSupélec, CNRS, SPMS, 91190, Gif-sur-Yvette, France & Université Paris-Saclay, CentraleSupélec, ENS Paris-Saclay, CNRS, LMPS - Laboratoire de Mécanique Paris-Saclay, 91190, Gif-sur-Yvette, France.

³ Université de Poitiers, CNRS, ENSMA SP2MI, 86962 Futuroscope-Chasseneuil, France

⁴ Helmholtz-Zentrum-Berlin für Materialien und Energy Gmbh, Institute “Functional Oxides for Energy Efficient Information Technology”, 14109 Berlin, Germany

⁵ Université Paris-Saclay, UVSQ, CNRS, ILV UMR8180, 78035, Versailles, France


⁶ Université Paris Diderot, CNRS, ITODYS UMR7086, 75013, Paris, France

⁷ Univ Rennes, CNRS, ISCR UMR6226, ScanMAT – UAR2025, 35000, Rennes, France


Keywords: DLI-ALD, Anatase TiO₂, Nanosheets, Ellipsometry

Corresponding authors

Dr. Bruno Bérini ; Université Paris-Saclay, UVSQ, CNRS, GEMaC, 45 avenue des Etats-Unis, 78035, Versailles, France.

 orcid.org/0000-0002-9063-5194 – Email : bruno.berini@uvsq.fr

Pr. Yves Dumont ; ; Université Paris-Saclay, UVSQ, CNRS, GEMaC, 45 avenue des Etats-Unis, 78035, Versailles, France.

 orcid.org/0000-0002-0739-428X – Email : yves.dumont@uvsq.fr

ABSTRACT

TiO₂ ultrathin films are required in many material research areas. The anatase phase was found to be more stable in case of atomic layer deposition growth, nevertheless a critical thickness of around 10 nm appears necessary to obtain crystallization on native silicon oxide on Si (001). This work focuses on direct liquid injection Atomic Layer Deposition (ALD) of TiO₂ films with thicknesses about some nanometers, using titanium tetra-isopropoxide as precursor and H₂O as oxidant. A particular care to the treatment of ellipsometric measurements is employed. Below the threshold value, films remain amorphous unless the growth starts onto a crystallized surface, . a thick TiO₂ layer in our case. Here we propose and show the efficiency of 2-dimensional (2D) [Ca₂Nb₃O₁₀]⁻ and [Ti_{0.865}O₂]^{0.54-} nanosheets as seeds at the surface for the crystallization and epitaxy of ultra-thin films of TiO₂ below the critical thickness. Furthermore, we show that the structure of the 2D nanosheets determines the growth orientation of the epitaxial anatase, namely (010) for [Ti_{0.865}O₂]^{0.54-}, and (100) for [Ca₂Nb₃O₁₀]⁻. These results, based on the tailoring of crystal anisotropy *via* adapted 2D seed nanosheets and low temperature ALD, opens the way for opto-electronics applications of titanium oxide layers of a few unit cells.

1. Introduction

TiO₂ is known to exist naturally in several polymorphs, named rutile, anatase and brookite. Both anatase and brookite are metastable and transform into rutile at temperatures above 600°C[1]. Anatase phase is mainly obtained from Atomic Layer Deposition (ALD) growth independently of the substrate (thermal SiO₂, RCA cleaned Si, Al₂O₃, buffer SrTiO₃)[2,3]. The substrate mainly plays a role on the crystallized grain size[2]. Rutile phase becomes prominent when films are obtained at temperatures above 350 °C[4] after annealing[5]. Kim *et al.* also grew the rutile phase on a Ru electrode by varying the O₃ high concentration while the deposition under the same conditions on Si wafer or Pt electrode leads to the anatase phase[6]. The surface energy allows the control of the grain size in low thermal budget processes [2,7]. For physical vapor deposition technique as pulsed laser deposition, it has been shown that the substrate orientation could promote either the anatase phase onto (100)SrTiO₃, (110) and (100)LaAlO₃ or the rutile phase onto (111)SrTiO₃[8]. The oxygen pressure is also a key parameter to favor the rutile phase (at low PO₂ < 0.1 mTorr) or anatase phase (at high PO₂ > 5mTorr). The brookite phase has been obtained between these two values[9] but also appeared for larger film thicknesses (45-65 nm) after a transformation from the anatase phase [10]. An oxygen deficiency content during the growth is also necessary for the formation of brookite or rutile from RF-sputtered films[11]. TiO₂ is a technological material used in numerous applications, more particularly as a high-k dielectric in next generation memory devices[12] or in nanophotonic structures and devices[13]. This oxide has very good photocatalytic quality[14,15] and is also employed as a coating layer for silicon solar cells[16]. These functionalities are strongly correlated to its microstructure and many efforts are made in surface engineering to control crystallization and grain size.

Atomic Layer Deposition (ALD) is a sequential thin film deposition technique where injections of metal precursor and oxidant are temporally separated by purge times[17,18]. This method is known for its very high precision in controlling the thickness of thin films through the number of cycles with an excellent uniformity for flat surface as in the present case, provided that the conditions of the so-called “ALD window” deposition are applied. The ALD window corresponds to a self-limiting saturated growth regime resulting in a constant growth rate (GPC for growth per cycle) independent of the temperature or the amount of precursor or oxidant. In this case, saturation curves are made to know the quantities to be injected and to establish the type of regime, i.e. an unsaturated or a saturated regime[19]. Consequently, one other important

advantage of ALD compared to other deposition techniques is the great conformality with a constant thickness for all sample morphologies. Nevertheless, these remarks are often mitigated as the chemical precursor/surface interactions are preponderant which might result in non-linear layer thickness evolution as a function of the number of cycles at the first stage of growth. The size of the molecules also plays a significant role[2]. In the case of titanium dioxide (TiO_2), several authors have observed a change in the deposition rate associated with a sudden crystallization [20–23]. This has a direct impact on the quality of the thin layers and thus in the materials properties.

Moreover, ALD deposition temperatures are dependent on the chosen precursors. There is a wide choice for titanium precursors with different reactivity but each has its own limitations. Indeed, among them, halides precursors produce HCl while organometallic ones tend to decompose at temperatures below 300°C [24,25,18,26]. Moreover, new precursors such as Prime Ti and Star Ti have been developed to overcome these issues which allow deposits to be grown at 325°C and 400°C , respectively[27]. Several oxidants are also available depending on the nature of precursors. H_2O and O_3 are compatible with the titanium tetra-isopropoxide (TTIP) used in this study[28]. For H_2O , it is considered that the hydroxyl groups are the reactive sites for chemisorption, and that the surface carbonates are the reactive sites for O_3 [29,30].

Herein, we are interested in the growth of TiO_2 on native oxidized Si (i.e. with the native oxide on the top of around 2nm) by Direct Liquid Injection Atomic Layer Deposition (DLI-ALD), focusing our attention on the aspects of crystallization at low numbers of cycles (first stages of the growth). The direct liquid injection ALD (DLI-ALD) is a particular case of ALD process where the chemical precursor is diluted in a solvent used as liquid carrier rather than taking saturated vapors from bubblers system. The mixture is then vaporized and transported into the deposit chamber. The Direct Liquid Injection vaporizers provide a perfect control of precursor flow and even allow utilization of low vapor pressure and diluted chemical precursors. In order to promote the crystallization of TiO_2 films deposited on Si and their local epitaxy, we looked at the effect of oxide nanosheets (NNS) as buffer layers. NNS have been known for about 15 years to induce the crystallization and the preferential orientation of thin films grown on various substrates such as silicon, glass, mica, polymer, ..., by different methods of growth (pulsed laser deposition, sputtering, sol-gel)[31–35]. These NNS are obtained by a top-down approach consisting of an exfoliation of the parent layered phase, itself synthesized by solid state reaction method or by reaction in molten salts. After their transfer to the substrate, the NNS are aimed

to act as seeds for the growth of the subsequent deposited thin film. Indeed, a local epitaxy of anatase TiO₂ might be reached if a small lattice mismatch exists with the NNS two-dimensional crystal lattice. Here, we used [Ca₂Nb₃O₁₀]⁻ (NNS-CNO) and [Ti_{0.865}O₂]^{0.54-} (NNS-TO) nanosheets, which have respectively: square lattice parameters $a_{CNO} = b_{CNO} = 3.85 \text{ \AA}$, and rectangular lattice parameters $a_{TO} = 3.82 \text{ \AA}$ and $c_{TO} = 2.97 \text{ \AA}$ close to the ones of crystalline TiO₂ anatase tetragonal phase: $a_{TiO_2} = b_{TiO_2} = 3.785 \text{ \AA}$ and $c_{TiO_2} = 9.514 \text{ \AA}$ (space group: *I4₁/amd*). Structural properties of ALD TiO₂ films deposited on uncovered and on NNS-covered silicon substrates are here investigated and compared by the conjunction of X-ray photoemission spectroscopy, spectroscopic ellipsometry, high-resolution transmission electron microscopy and in-plane high resolution X-ray diffraction.

2. Materials and methods

TiO₂ films were grown on as received two inches (100)Si substrates by DLI ALD/CVD setup (ANNEALSYS Inc. MC50 reactor) equipped with 4 pulsed direct liquid injectors (DLI for Kemstream Inc.) allowing an extremely fine nebulization of precursor mixture as shown in reference[36]. The growth chamber is a quartz tube surrounded by 8 halogen infrared lamps allowing a temperature range from room temperature to 1100°C. The deposition temperatures were varied between [200-295°C]. The chamber pressure was around 5×10^{-2} Torr. Ti precursor was prepared in a glove box from TTIP [(Ti(O-ⁱPr)₄)] (STREM Inc.) dissolved in toluene with a concentration of 7.5×10^{-3} M. This precursor solution was kept in a vessel under 4 bars of N₂ gas (5N purity) at room temperature. Vaporizer head temperature was fixed to 110°C. H₂O vapor was used as co-reactant. Deionized water was maintained in a dedicated vessel at room temperature. For all growths, we proceed to 10 x H₂O injection/purge cycles at the growth temperature in order to prepare the surface.

Synthesis of [Ca₂Nb₃O₁₀]⁻ (NNS-CNO) oxide nanosheets: the layered KCa₂Nb₃O₁₀ parent phase was synthesized by solid state reaction in an alumina crucible by firing mixtures of K₂CO₃ (with a 20 mol. % excess, Acros Organic 99%), Ca₂CO₃ (Sigma-Aldrich 99.95%) and Nb₂O₅ (Alfa Aesar 99.5%) at 1100°C in air for 10 h[31,37]. The precursors were previously ball-milled for 5 h in ethanol. The excess of K₂CO₃ was added to compensate the depletion of volatile potassium at high temperature. After reaction, the obtained powder was filtered and washed three times, and dried at 70°C. The powder was then protonated by ion-exchange in a 6 M

HNO₃ (Sigma-Aldrich) solution at room temperature for 3 days, with daily replacement of the acid. HCa₂Nb₃O₁₀ (HCNO) powder was filtered and washed 3 times, and dried. The exfoliation of HCNO was carried out by stirring the powder in a tetra-n-butylammonium hydroxide (TBAOH) (Thermo Scientific) solution with a HCNO/TBAOH 1:1.8 molar ratio. Monolayer of NNS-CNO were deposited on silicon substrate (Crystec GmbH) by drop-casting method[38] 120 μL of the CNO solution was diluted into 15 mL of ultrapure H₂O with 600 μL of ethanol. A 70 μL drop of this suspension was loaded with a pipet on the substrate heated on a hot plate at 100°C, and immediately removed by the pipet.

Synthesis of [Ti_{0.865}O₂]^{0.54-} (NNS-TO) oxide nanosheets: the layered K_{0.8}Ti_{1.73}Li_{0.27}O₄ parent phase was synthesized by molten salt method, using K₂MoO₄ as salt[38] K₂CO₃, (Acros Organic 99%), TiO₂ (Alfa Aesar 99.8%), Li₂CO₃ (Sigma-Aldrich 99%), and MoO₃ (Alfa Aesar 99.95%) were weighted in a molar ratio of 1.67:1.73: 0.13:1.27, ball-milled for 5h in ethanol and then fired in a platinum crucible at 1200°C for 10h. The K₂MoO₄ salt was formed in the mixture by reaction between K₂CO₃ and MoO₃. The layered phase was protonated similarly to KCNO in 1 day. Exfoliation was carried out in a TBAOH solution with a powder/TBAOH 1:1 molar ratio. The nanosheets were drop-casted on heated (100°C) silicon substrate by using a mixture of 150 μL of parent solution, 15 mL of ultra-pure water, and 1.2 mL of ethanol.

Both types of NNS-covered Si samples were placed after drop-casting in an UV ozone cleaner for 30 minutes, and finally in an oven for 1 h at 110°C.

Ellipsometric measurements were systematically carried out in the range 370-1690 nm between 50-70° incident angles with a commercial spectroscopic ellipsometer (WOOLLAM M2000) after deposition. The thickness is among the most relevant parameters of ALD process. Indeed, to determine the growth rate or growth per cycle (GPC), the final thickness is divided by the number of ALD cycles. The curve GPC as function of the temperature gives the self-limiting ALD conditions e.g. the well-known ALD window. Lot of care should be brought for the modelling because deviation in optical indexes can be compensated by the thickness evaluation. Moreover, ellipsometric parameters are very sensitive to the stoichiometry, phase transition and even surface contamination[39,40]. Thickness, refractive index (n) and absorption coefficient (k) can be extracted through model-based analysis of the experimental data. Here, we used a simple four layers stacking model consisting of a Si substrate with a SiO₂ native layer[41]. From as received substrate, SiO₂ thickness was found to be 2.3 nm. It has been confirmed by high resolution transmission electronic microscopy (HRTEM), and we fixed this value for all the samples. A Cauchy layer is used as optical dispersion model commonly used for

determining the optical constants of a transparent or partially transparent film as TiO₂[42] in the 370-1690 nm wavelength range and a Bruggeman effective medium approximation (BEMA) model simulated the surface roughness. The first approach is to fix the optical indexes from a sample where the thickness is measured elsewhere.

Spectroscopic ellipsometry in the visible to UV range (211-800 nm) has also been performed on a distinct ellipsometer (also WOOLLAM M2000 but with UV range) for selected samples. The real and imaginary parts of the optical indices (n,k) of the TiO₂ layer are obtained by fitting a four-layer model onto the measured ellipsometric data as detailed in the supplementary information. The optical indices of TiO₂ are fitted using a dispersion model comprising one or several Tauc-Lorentz oscillators with a common energy gap.

The surface morphologies were examined by Atomic Force Microscopy (AFM) (BRUKER Dimension ICON) operating in Peak Force mode with commercial ScanAsyst-Air tip.

Grazing incidence X-ray diffraction (GIXRD) and X-ray reflectivity (XRR) measurements were performed on an Empyrean diffractometer (@Malvern-Panalytical), with a similar configuration. The source is a filtered copper tube ($K_{\alpha} = 1.541874 \text{ \AA}$) and a parallel plate collimator (0.27°) is placed before the Pixcel multi-channel detector. By using a very small divergence slit ($1/32^{\circ}$), the beam is then considered parallel. A 5-axis cradle allows perfect positioning of the height and inclination of the sample. For the GIXRD measurements: ω , the incidence angle, is fixed at 1° , the scan range goes from 15 to 90° in 2θ , with a step size of 0.06° and a time per step of 6 s. The XRR measurements is an ω - 2θ scan from 0.2° to 1.4° , with a 0.003° step size during 1 s.

In-plane X-ray diffraction (XRD) was carried out using a 3 kV Smartlab Rigaku instrument working with a Cu- $K_{\alpha 1,2}$ radiation and equipped with a Hypix detector. 0.5° in-plane parallel collimator (PSC) and analyzer optics (PSA) were used. Scans were recorded with a beam incidence of 0.3° . The scan range was 15 - 75° in $2\theta_{\gamma}/\varphi$, with a step size of 0.016° and a speed of $1.2^{\circ}/\text{min}$.

5 nm thick films grown on NNS-CNO/Si and NNS-TO/Si were characterized by HRTEM. Cross-section TEM samples were prepared on a FEI ThermoFisher Helios Nanolab 660 by using the standard lift-out technique, and were characterized by using a FEI Titan3 G2 80-300 microscope, operated at 300 kV and equipped with a Cs probe corrector. Images were acquired in high-resolution mode in TEM and scanning TEM (STEM) modes. Plane-view samples were

prepared by scratching the film surface with a diamond tip; obtained film fragments were then collected on a commercial holey carbon-coated copper microgrid Cu grid. These samples were characterized with a JEOL 2100 instrument operating at 200 kV and equipped with a Gatan Orius 200D camera.

X-ray Photoelectron Spectroscopy (XPS) analyses were conducted on a Thermofisher Scientific Escalab 250 xi spectrometer equipped with a monochromated Al-K α anode (1486.6 eV). Both survey and core level spectra were recorded with a 650 μ m spot size. The photoelectron detection was performed, normal to the surface, using a constant analyzer energy mode (10 eV pass energy) and a 0.1 eV energy step. XPS depth profiling required the use of the Thermofisher Scientific MAGCIS dual-beam ion gun. Monoatomic Argon (Ar⁺) ions were accelerated to reach the sample with a kinetic energy of 1000 eV and an angle of 30° from the surface normal. The ion beam raster width was set to 1 mm. Quantification was performed based on the O1s, C1s, Ti2p and Si2p photopeak areas after a Shirley type background subtraction using the Thermofisher Scientific Advantage© software and its “ALTHERMO1” library as sensitivity factor collection.

3. Results and discussion

3.1. TiO₂ growth as function of the temperature. The first step consists in determining the ALD window, i.e. a self-saturated growth regime which does not depend on the temperature. This ALD window should be taken as an indication because many phenomena can mask it or, conversely, suggest that a plateau in the GPC curve as a function of temperature really corresponds to such window[43]. A same metallic precursor/oxidant couple generally leads approximately to the same plateau value independently of the instrument. Figure 1.a. shows the ALD windows of TiO₂ films with conditions as following: for the 300 cycles ALD windows, the parameters were set to 35 ms for the duration of the TTIP pulse followed a 15 s purge and 10 ms for the H₂O pulse followed by a 15 s purge. For the 1200 cycles ALD windows, the parameters were set to 45 ms for the duration of the TTIP pulse followed by a 20 s purge and 15 ms for H₂O pulse followed by a 20 s purge. The pressure was set at 1.2 Torr using a constant N₂ flow rate of 300 sccm. Preliminary test showed that a plateau is already reached from the lowest parameters of TiO₂ injection time (35 ms) used in the 300 cycles experiments. Two distinguishable GPC were found: 0.023 nm/cycle for the 300 cycles experiments and

0.03 nm / cycle for the 1200 cycles experiments. This second value is in good agreement with the literature[3,28,44–48]. An explanation for the 0.022 nm/cycle GPC will be given later in the text. GIXRD measurements were carried out on thickest layers, corresponding to 1200 cycles, prepared at 200, 230, 240 and 295°C and confirm that TiO₂ anatase form is obtained (figure 2). The thicknesses extracted from XRR measurements (figure S11 and Table S11) are close to the ones obtained by ellipsometry where the precision is linked to a good knowledge of the optical indices. The signal loss with the temperature is related to an increased roughness. AFM images clearly show a change in morphology (figure 3) with initial small grains associated with a low roughness (1 nm), followed by the development of larger crystallites that look like “cabbage leaves “ also observed elsewhere[7,22,49], and then by a reduction of crystallites size resulting in a significant roughness increase. These observations are summarized in figure 1.b where the calculated root mean square (RMS) roughness is plotted as a function of the deposition temperature for 1200 cycles samples. It is interesting to note that the shape of the curve is very similar to the one obtained for the ALD window with a RMS plateau at 2.3 nm in the temperature range [220-250°C].

3.2. TiO₂ growth as function of number of cycles. The thickness was plotted as a function of the number of cycles for deposits under standard conditions (TTIP 45 ms/ Purge 20 s/ H₂O 15 ms/ Purge 20 s) at 240°C (see figure 4). An inflexion point around 500 cycles corresponding to a thickness of about 10 nm is observed. This is consistent with previous observations of two distinct slopes as a function of number of cycles n.[2,3,20,22,23] We obtain approximately the same number of cycles as Rich *et al.*[23] but with half the thickness of their films. Some samples presented by red points on the graph correspond to a new growth on samples previously made: for 300 cycles (100 + 200 cycles), 400 cycles (100 + 300 cycles), 900 cycles (400 + 500 cycles), 1500 cycles (600 + 900 cycles). The first three points coincide with the samples made in one step. Nevertheless, for the 600 + 900 cycles sample, it can be seen that this point deviates from the black line representing the second GPC slope beyond 500 cycles. This can be explained if we take into consideration that this sample is the addition of two deposits with the highest GPCs, i.e. from a sample beyond 500 cycles and a new growth beyond 500 cycles. AFM images of the samples are shown in figure 5 and we clearly see a correspondence between the change in slope and the appearance of crystallites from 500 cycles with this “cabbage leaves” morphology already observed in the previous temperature study. When plotting the RMS as a function of the number of cycles or of the thickness (figure 4.b), we clearly distinguish two tendencies: a first one with a number of cycles < 500 where the

roughness is almost constant and of the order of 0.4 nm, and a second with a clear change from 500 cycles and a linear increase in roughness with the number of cycles (or thickness). Several explanations have been proposed in the literature, incriminating an O₂ deficit for Chiappim *et al.*[22] with fully stoichiometric TiO₂ beyond 400 cycles, or a transition from an amorphous to crystallized state for others authors. In the Rich's study[23], an increase of density is clearly shown starting from a thickness of 10 nm. Purunen *et al.*[2] has proposed a simplified scheme for the growth: TiO₂ growth begins as an amorphous film and after a certain thickness, crystallite nuclei form randomly at the surface. The thickness at which this occurs and the density of the nuclei depend on growth characteristics and temperature. It is worth noting that it is possible to accelerate the growth of crystallites by adding dopants such as Nb₂O₅ or Ta₂O₅[14]. The nature of the substrate also plays a role in the formation of crystallites: this is the case of a deposit onto Al₂O₃ compared with SiO₂[2] where the crystallization can be obtained from 200 cycles but at a temperature of 300°C. Comparing the growth of TiO₂ onto Al₂O₃, HfO₂ and Pt, Cho *et al.*[7] concludes that the grain sizes are controlled by the surface energy without changing the kinetic energy i.e. keeping a low thermal budget.

3.3. Focus on ellipsometric measurements and annealing effect. (see also the SI for more details). The onset of crystallization around 500 cycles is also evidenced by investigating the optical properties. The optical indices (n,k) of the TiO₂ layer are displayed in figure 6 for a new series of samples grown with 300 cycles (sample B), 720 cycles (samples C), and 1200 cycles (sample D) with the following conditions (TTIP 45 ms/ Purge 20 s/ H₂O 15 ms/ Purge 20 s) at 240°C. Samples were annealed in the ANNEALSYS Inc. MC50 reactor with the conditions of B. Rich *et al.*[23], i.e. at 500°C for 10 min in a N₂ atmosphere (flow of 300 sccm corresponding to a pressure of 8.6×10^{-1} Torr). Details of the series is reported in table 1. For sample B with or without thermal annealing, the optical indices of the TiO₂ layer are nicely reproduced by a dispersion model comprising a single Tauc-Lorentz oscillator. This is further evidence of the amorphous nature of TiO₂ at 300 cycles, as the Tauc-Lorentz dispersion model is characteristic of amorphous materials with bandgap in the region of interest (and was originally designed for this purpose)[50] and is indeed commonly used for amorphous TiO₂ in the literature.[42,51,52] The optical indices for sample B are comparable to those of amorphous TiO₂, reaching $n = 2.33$ at 550 nm.[51,53] After the thermal annealing, the indices increase strongly up to $n = 2.42$ at 550 nm, probably indicating an improvement in oxygen stoichiometry and/or a densification of the layer, which is consistent with a slight decrease in thickness from 5.4 nm to 5.1 nm upon thermal annealing as fitted by the ellipsometry modeling in the visible-UV range. However, it

maintains its amorphous nature: indeed, the absorption peak around 5 eV visible in the k spectrum (figure 6.b) remains notably broad and smooth, and a single Tauc-Lorentz oscillator is still sufficient to reproduce nicely its line shape. The energy gap of the Tauc-Lorentz oscillator is almost unchanged before ($E_g = 3.38$ eV) and after annealing ($E_g = 3.37$ eV): this value is consistent with the ones usually reported for amorphous TiO_x , ranging from 3.3 to 3.5 eV[51,54–57].

From there, increasing the number of cycles produces a noticeable and continuous increase of the optical index n in the visible range, namely up to $n = 2.42$ and $n = 2.55$ at 550 nm for 720 cycles (sample C) and 1200 cycles (sample D), respectively. These values are consistent with those of anatase TiO_2 [58] present in the films, in agreement with XRD results. Regarding the k spectrum in the UV range (figure 6.b), the absorption peaks of samples C and D show a more complex structure than sample B: the broad and smooth absorption peak of the amorphous TiO_2 gives way to a multiple set of thinner absorption peaks, which can be nicely reproduced by a set of Tauc-Lorentz oscillators with a common energy gap around 3.1 eV (sample C) and 3.2 eV (sample D), as detailed in the supplementary information. This multi-peaks structure evidences a clear (potentially partial) crystallization of the TiO_2 , consistent with the conclusions of XRD measurements. The values of E_g are consistent with $E_g = 3.2$ eV of single-crystal anatase TiO_2 [59] and the slight decrease of E_g upon crystallization observed here converges with previous reports on ALD TiO_2 films[51,54]. What is more, the centering energies of the Tauc-Lorentz oscillators are consistent with the absorption spectrum of anatase TiO_2 along the ordinary axis for the peaks around 4 and 5 eV, and along the extraordinary axis for the peak around 4.5 eV[58]. The maximum value of $k = 1.7$ reached around 5 eV for samples C and D is also consistent with anatase TiO_2 . Confirming the XRD measurements, these observations allow to rule out the presence of rutile TiO_2 , as the latter reaches much higher maximum $k = 3.0$ value at 4.5 eV, as well as higher $n = 2.9$ at 550 nm as compared to anatase TiO_2 . As samples C and D are *a priori* not noticeably textured, the exact line shape of the k spectrum may include contributions of both the ordinary and extraordinary components of the anatase TiO_2 , and therefore may be very sensible to the orientation of the anatase TiO_2 grains, which may explain easily the slight differences between the k spectra of the samples C and D in the UV range.

Strikingly, thermal annealing at 500°C on these samples C and D does not modify their optical indices. That is, they are already fully crystallized and the thermal annealing does not provide any further increase of modification of n and k .

3.4. TiO₂ growth onto TiO₂/SiO₂/Si pseudo substrates. The crystalline form of TiO₂ has many advantages including a higher refractive index than the amorphous form as seen before. In order to highlight the influence of the substrate, we focus now into samples whose growth was carried out in two separate steps exploiting the 2 inches size of our sample holder (cf. table 1). It is worth to indicate that the (100)Si substrates are untreated (e.g. with the presence of the native oxide SiO₂ layer). TEM analysis confirms that the 300 cycles sample (sample B) is amorphous while the 720 cycles sample (sample C) is polycrystalline (Figure 7) in accordance with XRD measurements. A good correspondence is obtained between the determination of the respective thicknesses by ellipsometry and TEM in these heterostructures.

XPS analysis have been performed on the different samples to control the chemistry and local environments of the ALD-grown titanium oxides. The Ti2p, Si2p, O1s and C1s spectra obtained on the 300 cycles sample (sample B) are given in supporting information (fig. SI12). They confirm the deposition of a TiO₂ thin layer. Indeed, the silicon substrate is detected which indicates that the entire oxide layer is probed and corroborates a thickness below 10 nanometers. The shape and position of the Ti2p photopeaks correspond to a chemical environment of Ti⁴⁺. Furthermore, the quantitative analysis gives an O/Ti ratio around 2. XPS depth profiling (Ar⁺ 1000 eV, high current, raster 1 mm) was necessary to probe thicker layers. One crucial information for ALD-growth layer is obtained with the C1s peak only detected at the beginning of the sputtering which shows that no ALD precursors remain incorporated inside the oxide layer (efficient decomposition/elimination during the process). This observation is consistent with the recent Dufond *et al's* . study that stated a threshold temperature of 200°C for ligand free TiO₂ thin films with TTIP/H₂O couple.[60] The O/Ti ratio is slightly reduced in the bulk of the layer upon sputtering, which is related to a beam effect generating a partial reduction of TiO₂ layers. Consequently, based on these results, the hypothesis of an oxygen deficiency being the cause of non-crystallization for a number of cycles lower than 500 can be ruled out.

Even more interesting is the situation of “sequential layer growths”. The sample E (300 cycles + 720 cycles) has been prepared by applying 720 new cycles simultaneously, both onto a piece of sample B and onto a new SiO₂/Si substrate which leads to the sample C (720 cycles). The TEM cross-section images clearly show two distinct areas corresponding to the two deposits. The area close to the silicon substrate, corresponding to the deposit obtained with the first 300 cycles, remains amorphous while the second one corresponding to the deposit grown during the 720 cycles is crystallized. Conversely, the sample F has been obtained by depositing a layer

corresponding to 300 cycles on a sample where a crystallized deposit was previously grown by 720 cycles (sample A). Interestingly, the entire TiO_2 layer is crystallized in that case which indicates that the first crystalline layer has clearly favored the growth of the subsequent second crystalline layer, even for a few nanometers. The same recipe is followed for sample E except that the second layer is obtained with 720 cycles. This sample is also fully crystallized which confirms that the crystalline growth is highly privileged by using a pseudo-crystalline substrate.

3.5. TiO_2 growth onto nanosheets/ SiO_2/Si pseudo substrates. We have seen previously and in the literature that it is possible to obtain crystallization starting from a crystallized substrate with similar lattice parameters. We are thus interested in this part in the deposition of TiO_2 onto NNS-TO and NNS-CNO nanosheets covering a large substrate surface (about $10 \times 20 \text{ mm}^2$). A major advantage is the possibility of depositing these NNS on any type of substrate such as Si and glass. The low thickness of this layer of nanosheets ($\sim 0.4 \text{ nm}$ for NNS/TO and $\sim 1.5 \text{ nm}$ for NNS/CNO) also allows their good visible light transmission as demonstrated recently by Boileau *et al.*[61] with the deposition of transparent conductor oxides SrVO_3 and CaVO_3 on NNS-CNO. For purpose of comparison with the previous samples, the NNS were deposited on untreated (100)Si substrates by the drop casting technique[62]. AFM images of NNS on SiO_2/Si are given in figure SI13 and show an excellent covering of the substrate. Figure 8 presents the AFM images after 300 and 1000 cycles of TiO_2 onto SiO_2/Si , NNS-TO and NNS-CNO. For the 300 cycles of TiO_2 onto both types of NNS, the roughness is slightly higher (1.2 nm) corresponding to the roughness of the NNS onto SiO_2/Si (see figure SI13). Surprisingly, for the 1000 cycles growth, the morphology of the TiO_2 layer is clearly different compared to those obtained after the direct growth onto SiO_2/Si but with a comparable roughness, suggesting another type of growth. XRR curves of these films are displayed in figures SI14a and SI14b and materials characteristics extracted from simulations are listed in table SI12. From these measurements, it comes that the thickness of the TiO_2 film is about 5 nm for 300 cycles, and about 26 nm for 1000 cycles. Figure 9a displays the in-plane XRD patterns of 26 nm thick TiO_2 films grown on Si, on NNS-TO and on NNS-CNO. In-plane XRD is a sensitive surface technique using a grazing incident beam and allowing to detect vertical crystallographic planes relatively to the sample surface. The film grown directly on SiO_2/Si is polycrystalline (blue curve), while the $\text{TiO}_2/\text{NNS-TO}$ film (green curve) presents a weak (010) out-of-plane preferential orientation revealed by the higher intensity of the in-plane 200 reflection at $2\theta\chi = 48^\circ$ and the absence of 220 reflection at $2\theta\chi = 70^\circ$. The thin NNS-TO ($\sim 0.4 \text{ nm}$) films are not detected in the pattern. The $\text{TiO}_2/\text{NNS-CNO}$ film (red curve) shows a stronger (002)

preferential orientation as indicated by the intense in-plane 200 and 220 reflections at $2\theta\chi = 48^\circ$ and 70° , respectively, while the other reflections (as 101, 004, 105, ...) are reduced. For this sample, the *hk0* reflections of the NNS-CNO are also observed (planes labeled in italics), due to the thickness of the nanosheets (~ 1.5 nm). Preferential orientations observed for films grown on nanosheets covered substrates indicate that both types of NNS induces local epitaxy of anatase film on Si. The figure 10 displays schemes of the structures of the three materials oriented according to the results enlighten by the above in-plane XRD characterizations. For (010) anatase film grown on NNS-TO (figure 10a), there is a small mismatch ($\delta = 1.02\%$) between the lattice parameters of anatase ($a_{\text{TiO}_2} = 3.785 \text{ \AA}$) and that of nanosheets ($a_{\text{TO}} = 3.824 \text{ \AA}$), and a larger one in the other direction ($\delta = -6.67\%$) corresponding to 3 cells for nanosheets ($3 \times c_{\text{TO}} = 8.919 \text{ \AA}$) to accommodate the anatase parameter $c_{\text{TiO}_2} = 9.5139 \text{ \AA}$. For (001) anatase film grown on NNS-CNO, the epitaxy is due to the small lattice parameters mismatch ($\delta = 1.67\%$) between both structures along both [100] and [010] directions with $a_{\text{CNO}} = b_{\text{CNO}} = 3.85 \text{ \AA}$, and $a_{\text{TiO}_2} = b_{\text{TiO}_2} = 3.785 \text{ \AA}$, as depicted in figure 10b. This last result was also obtained by Shibata *et al.* on a TiO_2 film synthesized by sol-gel on glass substrate[32].

Figure 9b displays the in-plane XRD patterns of 5 nm thick TiO_2 films grown on Si, on NNS-TO and on NNS-CNO. While there is almost no signal for the film directly grown on SiO_2/Si as expected, the patterns of the films grown on NNS-TO and NNS-CNO display the 200 peak of the anatase phase indicating that nanosheets promote also local epitaxy for 5 nm thick films. Thus, TEM was performed on cross-sections of both films synthesized on NNS, in order to deeper understand the stacking of TiO_2 on NNS-TO/(001)Si (Figure 11) and NSS-CNO/(001)Si (Figure 12). Both BF- and HAADF-STEM images show well-crystallized and about 5 nm thick TiO_2 crystallites, directly on top of nanosheets, themselves lying on amorphous SiO_2 native layer of constant thickness of 2.5 nm. Figures 12a,b show that there is only one monolayer of NNS-CNO lying on the substrate in the observed area, while one can observed one monolayer of NNS-TO in figure 11b, and locally a stack of several nanosheets in figure 11a. Electron diffraction pattern (EDP) (Figure 11c) shows Si reflections (in red) together with TiO_2 films reflections. Indexation of this pattern reveals a preferential orientation of the film along the [010] direction, and demonstrates therefore the texture of TiO_2 film along [001] of the silicon substrate induces by the NNS-TO. As the nanosheets are arranged randomly in the plane, only a few areas in the sample prepared by cross-section are oriented with respect to the electron beam in such a way that crystalline planes are observable in the high-resolution image. In figure 11.b, we see crystalline planes inclined with respect to the surface. The inter-reticular distance

of these planes is about 3.52 Å which corresponds to the (011) planes of the anatase phase. The corresponding EDP (figure 11b) shows the reflection of this family of planes, also inclined with respect to the normal to the surface. We therefore do not directly observe the planes of the crystallite which are parallel to the surface (these planes, although present, are not visible in the image) but inclined planes of a crystal preferentially oriented according to the [010] direction as indicated in the EDP. Concerning the film deposited on NNS-CNO, we observe in the STEM images a crystallite preferentially oriented according to the [001] direction as indicated by the interplanar distance of 2.39 Å. This result is confirmed by the EDP in which we see the 004 reflection of the TiO₂ film aligned with the 001 reflection of Si (in red), and with the 001 reflection of the NNS-CNO, attesting to excellent local epitaxy. The latter are also elongated along the normal to the surface, as shown by the inset in the figure. This is due to the strong anisotropy of the nanosheets which by Fourier transform gives elongated reflections in the direction orthogonal to the 2D plane.

Figure SI15 displays in plane-view TEM results performed on this sample. The bright field micrograph shows that the TiO₂ film is structured in domains with a lateral size of about 80 nm, corresponding to the size of the nanosheets located underneath. The EDP recorded on one of these domains displays single crystalline patterns along the [001] zone axes of TiO₂ and NNS-CNO. A slight inclination of the sample made it possible to visualize the reflections of the two phases and to highlight the epitaxial relationships between them, as described in figure 10b.

Consequently, our results showed that the crystallization of TiO₂ very thin films (300 cycles corresponding to ~5 nm) not observed on pristine SiO₂/Si, can be obtained with 2D nanosheet templates, driving consequently an oriented texture of the anatase film. Some other strategies have been followed to look in details the influence of the Si-based substrate on the ALD growth: (i) Thermal SiO₂, RCA cleaned Si, Al₂O₃/Si for Puurunen et al.[2] who proposed a scheme explaining what we observed for the growth of TiO₂ on SiO₂/Si, (ii) SrTiO₃-buffered (001) Si[3] where four unit cells are necessary to create a stable template and (iii) RCA or HF treated SiO₂/Si[63]. This last reference emphasized that the study had to be carried out for very low thicknesses (100 cycles or 2.5 nm in their case) to obtain more information on the substrate effect. Nevertheless, this direct growth of oriented crystalline layer remains challenging. In order to clarify whether the crystallization of anatase on the nanosheets observed in our work is due to the small lattice mismatch or the complex oxide nature of the NSS, a further step will be to grow 300 cycles ALD TiO₂ films with the same protocol on other oxides nanosheets such

as $[\text{K}_{4-x}\text{Nb}_6\text{O}_{17}]^{x-}$ or $[\text{Cs}_4\text{W}_{11}\text{O}_{36}]^{2-}$ and also on single-crystalline oxide substrates that will not exhibit epitaxial relationships with the TiO_2 film.

4. Conclusions

In this work, the growth of TiO_2 layers of different thicknesses onto SiO_2/Si substrates have been performed by DLI-ALD using TTIP and water as Ti precursor/oxidant couple, in the low substrate temperatures range of $[200^\circ\text{C}-295^\circ\text{C}]$. Various parameters have been studied and a particular focus on the possibility to obtain crystalline ultra-thin anatase layers have been developed. Several important points have been raised.

In the ALD process, we observed two different GPC before and after 500 cycles which correspond to an obtained thickness of around 10 nanometers. The change observed after 500 cycles was related to the spontaneous crystallization of the TiO_2 films around this thickness. We also demonstrated that this crystallization process can be monitored by the RMS roughness, measured thanks to a now routine AFM tool, and give an easy way to follow growth mechanism and to correlate the morphology of the surface with the GPC curves.

A great attention was paid on the fitting procedure of the ellipsometric measurements. The “Vis-NIR Cauchy” method does not allow to decorrelate n and the thickness in the transparent range: nevertheless, we have shown in this work that while fixing the value of n it is well suited for a systematic study. The results are confirmed by the “UV-vis dispersion model” method, which allows to also investigate the absorbing UV range: it succeeds in decorrelating n , k and the thickness for thick samples, but reaches its limits in the transparent range for thin samples (< 5 nm), although the use of a dispersion model allows to partially overcome this limitation. Finally, the “thin film inversion” model developed by Maudet *et al.*[64] allows to unambiguously decorrelate n , k and the thickness even for very thin films (< 5 nm). In the specific case of this work, as detailed in the supplementary information, it has confirmed the validity of the “Vis-NIR Cauchy” and “UV-vis dispersion model” that may thus be used as systematic characterization methods. This stress the precaution to put in the usual film thickness measurements by ellipsometry associated to ALD growths.

We validate two strategies to force the crystallized growth of ultrathin (< 10 nm) anatase TiO_2 by ALD at low temperature with the TTIP/ H_2O as Ti precursor/oxidant couple, on any substrate, such as oxidized silicon. First is to growth directly on anatase pseudo-substrate, but this requires a pre-existing anatase surface. And second is to cover the substrate surface by adapted oxide

nanosheets, which will act as seed centers in the crystallization process. Our study with $[\text{Ca}_2\text{Nb}_3\text{O}_{10}]^-$ and $[\text{Ti}_{0.865}\text{O}_2]^{0.54-}$ oxide nanosheets show clearly that epitaxy is reachable even during the first cycles of ALD growth with an adapted substrate, that induce a high crystalline texture of the deposited anisotropic tetragonal anatase layer.

This study gives an illustration of the use of seed 2D layers is really promising as it could be integrated on different substrates, including glass for instance and can monitor preferential crystalline orientations for anisotropic functional layers even at few nanometers thicknesses, in association with low temperature ALD, as industrial compatible conformal deposition technique.

Declaration of Competing Interest

The authors declare that they have no competing financial interest or personal relationships that could have appeared to influence the work reported in this paper.

Acknowledgments

This work is supported by a public grant overseen by the French National Research Agency (ANR) as part of the “Investissements d’Avenir” program (Labex NanoSaclay, reference: ANR-10-LABX-0035), within the flagship AXION: partial founding of ALD set-up and A.G. postdoctoral fellowship. ALD equipment was complementary financed by Ile de France region within the Domaine d’Intérêt Majeur DIM OxyMORE (O’GRAAL project). The authors acknowledge also financial support of the French National Research Agency in the framework of the POLYNASH project (ANR-17-CE08-0012). Moreover this work has benefited from the support of different platforms: ScanMAT (UAR 2025, University of Rennes -CNRS) for XRD and TEM; and French ANR within “Equipement d’Excellence” MatMéca (ANR-10-EQPX-37 grant) for a second part of electron microscopy experiments. Authors gratefully thank Jean-Manuel Decamps, from ANNEALSYS, for fruitful discussions and advices.

Appendix A. Supplementary material

Supplementary data to this article can be found online at ...

This Supplementary Information details complementary measurements and associated analysis performed on these series of TiO_2 layers studied in the work. First part compares, for the series

(1200 cycles TiO₂ films at different temperatures on SiO₂/Si substrates), the thickness deduced by XRR and by ellipsometric measurements, as-well as roughness by AFM and fitted from XRR measurements. The second part explains and details ellipsometric fits to deduce dielectric functions of TiO₂ anatase ultrathin films, especially the robust one developed by Maudet *et al.* to adjust independently optical constants and thickness. Third chapter gives complements on TiO₂ layers deposited on NNS-TO and NSS-CNO, with AFM topological mappings and associated roughness, XRR scans and deduced thickness and roughness. And the fourth part shows in-plane TEM image and the EDP demonstrating the perfect local epitaxy of TiO₂ anatase 5nm-thick layer on top of NNS-CNO.

References

- [1] D.A.H. Hanaor, C.C. Sorrell, Review of the anatase to rutile phase transformation, *J Mater Sci.* 46 (2011) 855–874. <https://doi.org/10.1007/s10853-010-5113-0>.
- [2] R.L. Puurunen, T. Sajavaara, E. Santala, V. Miikkulainen, T. Saukkonen, M. Laitinen, M. Leskelä, Controlling the crystallinity and roughness of atomic layer deposited titanium dioxide films, *J Nanosci Nanotechnol.* 11 (2011) 8101–8107. <https://doi.org/10.1166/jnn.2011.5060>.
- [3] M.D. McDaniel, A. Posadas, T. Wang, A.A. Demkov, J.G. Ekerdt, Growth and characterization of epitaxial anatase TiO₂(001) on SrTiO₃-buffered Si(001) using atomic layer deposition, *Thin Solid Films.* 520 (2012) 6525–6530. <https://doi.org/10.1016/j.tsf.2012.06.061>.
- [4] J. Aarik, A. Aidla, T. Uustare, V. Sammelselg, Morphology and structure of TiO₂ thin films grown by atomic layer deposition, *Journal of Crystal Growth.* 148 (1995) 268–275. [https://doi.org/10.1016/0022-0248\(94\)00874-4](https://doi.org/10.1016/0022-0248(94)00874-4).
- [5] J. Li, L. Hui, W. Zhang, J. Lu, Y. Yang, H. Feng, Scalable production of ultra small TiO₂ nano crystal/activated carbon composites by atomic layer deposition for efficient removal of organic pollutants, *Advanced Powder Technology.* 32 (2021) 728–739. <https://doi.org/10.1016/j.appt.2021.01.013>.
- [6] S.K. Kim, W.-D. Kim, K.-M. Kim, C.S. Hwang, J. Jeong, High dielectric constant TiO₂ thin films on a Ru electrode grown at 250 °C by atomic-layer deposition, *Appl. Phys. Lett.* 85 (2004) 4112–4114. <https://doi.org/10.1063/1.1812832>.
- [7] C.J. Cho, J.-Y. Kang, W.C. Lee, S.-H. Baek, J.-S. Kim, C.S. Hwang, S.K. Kim, Interface Engineering for Extremely Large Grains in Explosively Crystallized TiO₂ Films Grown by Low-Temperature Atomic Layer Deposition, *Chem. Mater.* 29 (2017) 2046–2054. <https://doi.org/10.1021/acs.chemmater.6b04090>.
- [8] R.J. Kennedy, P.A. Stampe, The influence of lattice mismatch and film thickness on the growth of TiO₂ on LaAlO₃ and SrTiO₃ substrates, *Journal of Crystal Growth.* 252 (2003) 333–342. [https://doi.org/10.1016/S0022-0248\(02\)02514-9](https://doi.org/10.1016/S0022-0248(02)02514-9).
- [9] J.S. Mangum, O. Agirseven, J.E.S. Haggerty, J.D. Perkins, L.T. Schelhas, D.A. Kitchaev, L.M. Garten, D.S. Ginley, M.F. Toney, J. Tate, B.P. Gorman, Selective brookite polymorph formation related to the amorphous precursor state in TiO₂ thin films, *Journal of Non-Crystalline Solids.* 505 (2019) 109–114. <https://doi.org/10.1016/j.jnoncrysol.2018.10.049>.
- [10] J.E.S. Haggerty, L.T. Schelhas, D.A. Kitchaev, J.S. Mangum, L.M. Garten, W. Sun, K.H. Stone, J.D. Perkins, M.F. Toney, G. Ceder, D.S. Ginley, B.P. Gorman, J. Tate, High-fraction brookite films from amorphous precursors, *Sci Rep.* 7 (2017) 15232. <https://doi.org/10.1038/s41598-017-15364-y>.

- [11] O. Agirseven, D.T. Rivella Jr., J.E.S. Haggerty, P.O. Berry, K. Diffendaffer, A. Patterson, J. Krebs, J.S. Mangum, B.P. Gorman, J.D. Perkins, B.R. Chen, L.T. Schelhas, J. Tate, Crystallization of TiO₂ polymorphs from RF-sputtered, amorphous thin-film precursors, *AIP Advances*. 10 (2020) 025109. <https://doi.org/10.1063/1.5140368>.
- [12] S.K. Kim, K.M. Kim, D.S. Jeong, W. Jeon, K.J. Yoon, C.S. Hwang, Titanium dioxide thin films for next-generation memory devices, *Journal of Materials Research*. 28 (2013) 313–325. <https://doi.org/10.1557/jmr.2012.231>.
- [13] M.R. Saleem, R. Ali, M.B. Khan, S. Honkanen, J. Turunen, Impact of Atomic Layer Deposition to Nanophotonic Structures and Devices, *Frontiers in Materials*. 1 (2014). <https://www.frontiersin.org/article/10.3389/fmats.2014.00018> (accessed March 7, 2022).
- [14] V. Pore, T. Kivelä, M. Ritala, M. Leskelä, Atomic layer deposition of photocatalytic TiO₂ thin films from TiF₄ and H₂O, *Dalton Trans.* (2008) 6467–6474. <https://doi.org/10.1039/B809953G>.
- [15] A. Wold, Photocatalytic properties of titanium dioxide (TiO₂), *Chem. Mater.* 5 (1993) 280–283. <https://doi.org/10.1021/cm00027a008>.
- [16] B.S. Richards, Comparison of TiO₂ and other dielectric coatings for buried-contact solar cells: a review, *Progress in Photovoltaics: Research and Applications*. 12 (2004) 253–281. <https://doi.org/10.1002/pip.529>.
- [17] R.L. Puurunen, A Short History of Atomic Layer Deposition: Tuomo Suntola's Atomic Layer Epitaxy, *Chemical Vapor Deposition*. 20 (2014) 332–344. <https://doi.org/10.1002/cvde.201402012>.
- [18] V. Miikkulainen, M. Leskelä, M. Ritala, R.L. Puurunen, Crystallinity of inorganic films grown by atomic layer deposition: Overview and general trends, *Journal of Applied Physics*. 113 (2013) 021301. <https://doi.org/10.1063/1.4757907>.
- [19] K.-E. Elers, T. Blomberg, M. Peussa, B. Aitchison, S. Haukka, S. Marcus, Film Uniformity in Atomic Layer Deposition, *Chemical Vapor Deposition*. 12 (2006) 13–24. <https://doi.org/10.1002/cvde.200500024>.
- [20] S.K. Kim, S. Hoffmann-Eifert, M. Reiners, R. Waser, Relation Between Enhancement in Growth and Thickness-Dependent Crystallization in ALD TiO₂ Thin Films, *J. Electrochem. Soc.* 158 (2010) D6. <https://doi.org/10.1149/1.3507258>.
- [21] M.D. McDaniel, A. Posadas, T.Q. Ngo, A. Dhamdhere, D.J. Smith, A.A. Demkov, J.G. Ekerdt, Epitaxial strontium titanate films grown by atomic layer deposition on SrTiO₃-buffered Si(001) substrates, *Journal of Vacuum Science & Technology A*. 31 (2012) 01A136. <https://doi.org/10.1116/1.4770291>.
- [22] W. Chiappim, G.E. Testoni, J.S.B. de Lima, H.S. Medeiros, R.S. Pessoa, K.G. Grigorov, L. Vieira, H.S. Maciel, Effect of Process Temperature and Reaction Cycle Number on Atomic Layer Deposition of TiO₂ Thin Films Using TiCl₄ and H₂O Precursors: Correlation Between Material Properties and Process Environment, *Braz J Phys.* 46 (2016) 56–69. <https://doi.org/10.1007/s13538-015-0383-2>.
- [23] B.B. Rich, Y. Etinger-Geller, G. Ciatto, A. Katsman, B. Pokroy, Retention of surface structure causes lower density in atomic layer deposition of amorphous titanium oxide thin films, *Phys. Chem. Chem. Phys.* 23 (2021) 6600–6612. <https://doi.org/10.1039/D1CP00341K>.
- [24] V. Sammelselg, A. Rosental, A. Tarre, L. Niinistö, K. Heiskanen, K. Ilmonen, L.-S. Johansson, T. Uustare, TiO₂ thin films by atomic layer deposition: a case of uneven growth at low temperature, *Applied Surface Science*. 134 (1998) 78–86. [https://doi.org/10.1016/S0169-4332\(98\)00224-4](https://doi.org/10.1016/S0169-4332(98)00224-4).
- [25] C.D. McClure, C.J. Oldham, H.J. Walls, G.N. Parsons, Large effect of titanium precursor on surface reactivity and mechanical strength of electrospun nanofibers coated with TiO₂ by atomic layer deposition, *Journal of Vacuum Science & Technology A*. 31 (2013) 061506. <https://doi.org/10.1116/1.4817718>.
- [26] M. Reiners, K. Xu, N. Aslam, A. Devi, R. Waser, S. Hoffmann-Eifert, Growth and Crystallization of TiO₂ Thin Films by Atomic Layer Deposition Using a Novel Amido Guanidinate Titanium Source

- and Tetrakis-dimethylamido-titanium, *Chem. Mater.* 25 (2013) 2934–2943.
<https://doi.org/10.1021/cm303703r>.
- [27] R. Katamreddy, V. Omarjee, B. Feist, C. Dussarrat, Ti Source Precursors for Atomic Layer Deposition of TiO₂, STO and BST, *ECS Trans.* 16 (2008) 113. <https://doi.org/10.1149/1.2979986>.
- [28] M. Ritala, M. Leskela, L. Niinisto, P. Haussalo, Titanium isopropoxide as a precursor in atomic layer epitaxy of titanium dioxide thin films, *Chem. Mater.* 5 (1993) 1174–1181.
<https://doi.org/10.1021/cm00032a023>.
- [29] V.R. Rai, S. Agarwal, Surface Reaction Mechanisms during Ozone-Based Atomic Layer Deposition of Titanium Dioxide, *J. Phys. Chem. C.* 112 (2008) 9552–9554.
<https://doi.org/10.1021/jp8028616>.
- [30] E.R. Cleveland, L. Henn-Lecordier, G.W. Rubloff, Role of surface intermediates in enhanced, uniform growth rates of TiO₂ atomic layer deposition thin films using titanium tetraisopropoxide and ozone, *Journal of Vacuum Science & Technology A.* 30 (2012) 01A150.
<https://doi.org/10.1116/1.3669522>.
- [31] K. Kikuta, K. Noda, S. Okumura, T. Yamaguchi, S. Hirano, Orientation control of perovskite thin films on glass substrates by the application of a seed layer prepared from oxide nanosheets, *Journal of Sol-Gel Science and Technology.* 42 (2007) 381–387.
<https://doi.org/10.1007/s10971-006-0200-z>.
- [32] T. Shibata, K. Fukuda, Y. Ebina, T. Kogure, T. Sasaki, One-Nanometer-Thick Seed Layer of Unilamellar Nanosheets Promotes Oriented Growth of Oxide Crystal Films, *Advanced Materials.* 20 (2008) 231–235. <https://doi.org/10.1002/adma.200701381>.
- [33] M. Nijland, S. Kumar, R. Lubbers, D.H.A. Blank, G. Rijnders, G. Koster, J.E. ten Elshof, Local Control over Nucleation of Epitaxial Thin Films by Seed Layers of Inorganic Nanosheets, *ACS Appl. Mater. Interfaces.* 6 (2014) 2777–2785. <https://doi.org/10.1021/am4052624>.
- [34] A.P. Dral, M. Nijland, G. Koster, J.E. ten Elshof, Film transfer enabled by nanosheet seed layers on arbitrary sacrificial substrates, *APL Materials.* 3 (2015) 056102.
<https://doi.org/10.1063/1.4921070>.
- [35] J.J. Manguelle, F. Baudouin, C. Cibert, B. Domengès, V. Demange, M. Guilloux-Viry, A. Fouchet, G. Poullain, Orientation control of Platinum electrode grown on silicon using [Ca₂Nb₃O₁₀]-nanosheets as seed layer., *Thin Solid Films.* 765 (2023) 139640.
<https://doi.org/10.1016/j.tsf.2022.139640>.
- [36] L. Avril, J.M. Decams, L. Imhoff, Pulsed Direct liquid Injection ALD of TiO₂ Films Using Titanium Tetraisopropoxide Precursor, *Physics Procedia.* 46 (2013) 33–39.
<https://doi.org/10.1016/j.phpro.2013.07.063>.
- [37] F. Baudouin, V. Demange, S. Ollivier, L. Rault, A.S. Brito, A.S. Maia, F. Gouttefangeas, V. Bouquet, S. Députier, B. Bérimini, A. Fouchet, M. Guilloux-Viry, Orientation control of KNbO₃ film grown on glass substrates by Ca₂Nb₃O₁₀-nanosheets seed layer, *Thin Solid Films.* 693 (2020) 137682. <https://doi.org/10.1016/j.tsf.2019.137682>.
- [38] T. Tanaka, Y. Ebina, K. Takada, K. Kurashima, T. Sasaki, Oversized Titania Nanosheet Crystallites Derived from Flux-Grown Layered Titanate Single Crystals, *Chem. Mater.* 15 (2003) 3564–3568.
<https://doi.org/10.1021/cm034307j>.
- [39] B. Berini, N. Keller, Y. Dumont, E. Popova, W. Noun, M. Guyot, J. Vigneron, A. Etcheberry, N. Franco, R.M.C. da Silva, Reversible phase transformation of La Ni O_{3-x} thin films studied in situ by spectroscopic ellipsometry, *Physical Review B.* 76 (2007).
<https://doi.org/10.1103/PhysRevB.76.205417>.
- [40] D. Hrabovsky, B. Berini, A. Fouchet, D. Aureau, N. Keller, A. Etcheberry, Y. Dumont, Strontium titanate (100) surfaces monitoring by high temperature in situ ellipsometry, *Applied Surface Science.* 367 (2016) 307–311. <https://doi.org/10.1016/j.apsusc.2016.01.175>.
- [41] C.M. Herzinger, B. Johs, W.A. McGahan, J.A. Woollam, W. Paulson, Ellipsometric determination of optical constants for silicon and thermally grown silicon dioxide via a multi-sample, multi-wavelength, multi-angle investigation, *Journal of Applied Physics.* 83 (1998) 3323–3336.
<https://doi.org/10.1063/1.367101>.

- [42] P. Eiamchai, P. Chindaudom, A. Pokaipisit, P. Limsuwan, A spectroscopic ellipsometry study of TiO₂ thin films prepared by ion-assisted electron-beam evaporation, *Current Applied Physics*. 9 (2009) 707–712. <https://doi.org/10.1016/j.cap.2008.06.011>.
- [43] H.H. Sønsteby, A. Yanguas-Gil, J.W. Elam, Consistency and reproducibility in atomic layer deposition, *Journal of Vacuum Science & Technology A*. 38 (2020) 020804. <https://doi.org/10.1116/1.5140603>.
- [44] H.J. Lee, T. Moon, C.H. An, C.S. Hwang, 2D Electron Gas at the Interface of Atomic-Layer-Deposited Al₂O₃/TiO₂ on SrTiO₃ Single Crystal Substrate, *Advanced Electronic Materials*. 5 (2019) 1800527. <https://doi.org/10.1002/aelm.201800527>.
- [45] T.J. Seok, Y. Liu, J.H. Choi, H.J. Kim, D.H. Kim, S.M. Kim, J.H. Jang, D.-Y. Cho, S.W. Lee, T.J. Park, In Situ Observation of Two-Dimensional Electron Gas Creation at the Interface of an Atomic Layer-Deposited Al₂O₃/TiO₂ Thin-Film Heterostructure, *Chem. Mater.* 32 (2020) 7662–7669. <https://doi.org/10.1021/acs.chemmater.0c01572>.
- [46] S.D. Standridge, G.C. Schatz, J.T. Hupp, Toward Plasmonic Solar Cells: Protection of Silver Nanoparticles via Atomic Layer Deposition of TiO₂, *Langmuir*. 25 (2009) 2596–2600. <https://doi.org/10.1021/la900113e>.
- [47] A. Kosola, M. Putkonen, L.-S. Johansson, L. Niinistö, Effect of annealing in processing of strontium titanate thin films by ALD, *Applied Surface Science*. 211 (2003) 102–112. [https://doi.org/10.1016/S0169-4332\(03\)00175-2](https://doi.org/10.1016/S0169-4332(03)00175-2).
- [48] L. Avril, S. Reymond-Laruinaz, J.M. Decams, S. Bruyère, V. Potin, M.C.M. de Lucas, L. Imhoff, TiO₂ anatase films obtained by direct liquid injection atomic layer deposition at low temperature, *Applied Surface Science*. 288 (2014) 201–207. <https://doi.org/10.1016/j.apsusc.2013.10.007>.
- [49] H.K. Chung, S.O. Won, Y. Park, J.-S. Kim, T.J. Park, S.K. Kim, Atomic-layer deposition of TiO₂ thin films with a thermally stable (CpMe₅)Ti(OMe)₃ precursor, *Applied Surface Science*. 550 (2021) 149381. <https://doi.org/10.1016/j.apsusc.2021.149381>.
- [50] *Spectroscopic Ellipsometry: Principles and Applications* | Wiley, Wiley.Com. (n.d.). <https://www.wiley.com/en-us/Spectroscopic+Ellipsometry%3A+Principles+and+Applications-p-9780470016084> (accessed January 20, 2023).
- [51] A. Jolivet, C. Labbé, C. Frilay, O. Debieu, P. Marie, B. Horcholle, F. Lemarié, X. Portier, C. Grygiel, S. Duprey, W. Jadwisienczak, D. Ingram, M. Upadhyay, A. David, A. Fouchet, U. Lüders, J. Cardin, Structural, optical, and electrical properties of TiO₂ thin films deposited by ALD: Impact of the substrate, the deposited thickness and the deposition temperature, *Applied Surface Science*. 608 (2023) 155214. <https://doi.org/10.1016/j.apsusc.2022.155214>.
- [52] F. Maudet, Nanostructured layers by oblique incidence deposition : Microstructure and optical properties correlations applicated to high-performance anti-reflection treatments in extended visible and infrared range, phdthesis, Université de Poitiers, 2018. <https://theses.hal.science/tel-02139079> (accessed January 20, 2023).
- [53] D. Saha, R.S. Ajimsha, K. Rajiv, C. Mukherjee, M. Gupta, P. Misra, L.M. Kukreja, Spectroscopic ellipsometry characterization of amorphous and crystalline TiO₂ thin films grown by atomic layer deposition at different temperatures, *Applied Surface Science*. 315 (2014) 116–123. <https://doi.org/10.1016/j.apsusc.2014.07.098>.
- [54] J. Aarik, A. Aidla, A.-A. Kiisler, T. Uustare, V. Sammelselg, Effect of crystal structure on optical properties of TiO₂ films grown by atomic layer deposition, *Thin Solid Films*. 305 (1997) 270–273. [https://doi.org/10.1016/S0040-6090\(97\)00135-1](https://doi.org/10.1016/S0040-6090(97)00135-1).
- [55] S. Ratzsch, E.-B. Kley, A. Tünnermann, A. Szeghalmi, Influence of the oxygen plasma parameters on the atomic layer deposition of titanium dioxide, *Nanotechnology*. 26 (2015) 024003. <https://doi.org/10.1088/0957-4484/26/2/024003>.
- [56] S.-J. Park, J.-P. Lee, J.S. Jang, H. Rhu, H. Yu, B.Y. You, C.S. Kim, K.J. Kim, Y.J. Cho, S. Baik, W. Lee, In situ control of oxygen vacancies in TiO₂ by atomic layer deposition for resistive switching devices, *Nanotechnology*. 24 (2013) 295202. <https://doi.org/10.1088/0957-4484/24/29/295202>.

- [57] K. Eufinger, D. Poelman, H. Poelman, R. De Gryse, G.B. Marin, Photocatalytic activity of dc magnetron sputter deposited amorphous TiO₂ thin films, *Applied Surface Science*. 254 (2007) 148–152. <https://doi.org/10.1016/j.apsusc.2007.07.009>.
- [58] G.E. Jellison, L.A. Boatner, J.D. Budai, B.-S. Jeong, D.P. Norton, Spectroscopic ellipsometry of thin film and bulk anatase (TiO₂), *Journal of Applied Physics*. 93 (2003) 9537–9541. <https://doi.org/10.1063/1.1573737>.
- [59] H. Tang, H. Berger, P.E. Schmid, F. Lévy, G. Burri, Photoluminescence in TiO₂ anatase single crystals, *Solid State Communications*. 87 (1993) 847–850. [https://doi.org/10.1016/0038-1098\(93\)90427-0](https://doi.org/10.1016/0038-1098(93)90427-0).
- [60] M.E. Dufond, M.W. Diouf, C. Badie, C. Laffon, P. Parent, D. Ferry, D. Grosso, J.C.S. Kools, S.D. Elliott, L. Santinacci, Quantifying the Extent of Ligand Incorporation and the Effect on Properties of TiO₂ Thin Films Grown by Atomic Layer Deposition Using an Alkoxide or an Alkylamide, *Chem. Mater.* 32 (2020) 1393–1407. <https://doi.org/10.1021/acs.chemmater.9b03621>.
- [61] A. Boileau, S. Hurand, F. Baudouin, U. Lüders, M. Dallochio, B. Bérini, A. Cheikh, A. David, F. Paumier, T. Girardeau, P. Marie, C. Labbé, J. Cardin, D. Aureau, M. Frégnaux, M. Guilloux-Viry, W. Prellier, Y. Dumont, V. Demange, A. Fouchet, Highly Transparent and Conductive Indium-Free Vanadates Crystallized at Reduced Temperature on Glass Using a 2D Transparent Nanosheet Seed Layer, *Advanced Functional Materials*. 32 (2022) 2108047. <https://doi.org/10.1002/adfm.202108047>.
- [62] Y. Shi, M. Osada, Y. Ebina, T. Sasaki, Single Droplet Assembly for Two-Dimensional Nanosheet Tiling, *ACS Nano*. 14 (2020) 15216–15226. <https://doi.org/10.1021/acsnano.0c05434>.
- [63] D.R.G. Mitchell, D.J. Attard, G. Triani, Transmission electron microscopy studies of atomic layer deposition TiO₂ films grown on silicon, *Thin Solid Films*. 441 (2003) 85–95. [https://doi.org/10.1016/S0040-6090\(03\)00877-0](https://doi.org/10.1016/S0040-6090(03)00877-0).
- [64] F. Maudet, C. Van Dijck, M.H. Raza, C. Dubourdieu, A fully automatized method for the unambiguous wavelength-by-wavelength determination of the thickness and optical property of a very thin film with a transparent range, (2023). <https://doi.org/10.48550/arXiv.2303.06918>.

Sample	starting surface	number of cycles	Total cycles	SE Thickness * (nm)	SE Thickness ** (nm)	TEM Thickness (nm)	Crystalline structure	AFM Roughness (nm)	Thermal annealing
A	SiO ₂	720	720	20.3			anatase	1.4	no
B	SiO ₂	300	300	5.4	5.4	3.7	amorphous	0.4	500°C/10min
C	SiO ₂	720	720	18.6	19	21.7	anatase	1.7	500°C/10min
D	SiO ₂	1200	1200	40.4	40.8		anatase	2.6	500°C/10min
E	Sample B	720	300+720	23.2		22.5	amorphous + anatase	1.6	no
F	Sample A	300	720+300	27.6		28.4	anatase + anatase	1.8	no
G	Sample A	720	720+720	43		43.4	anatase + anatase	3.3	no

Table 1

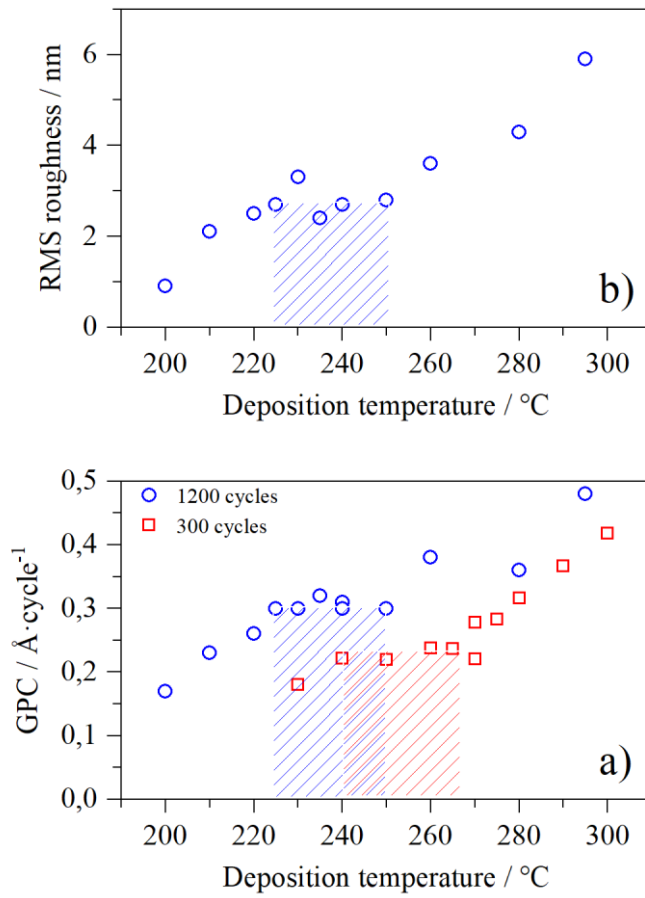


Figure 1: a) GPC as a function of deposition temperature for 300 (red squares) and 1200 cycles (blue circles) and b) AFM RMS roughness as a function of deposition temperature for samples with 1200 cycles.

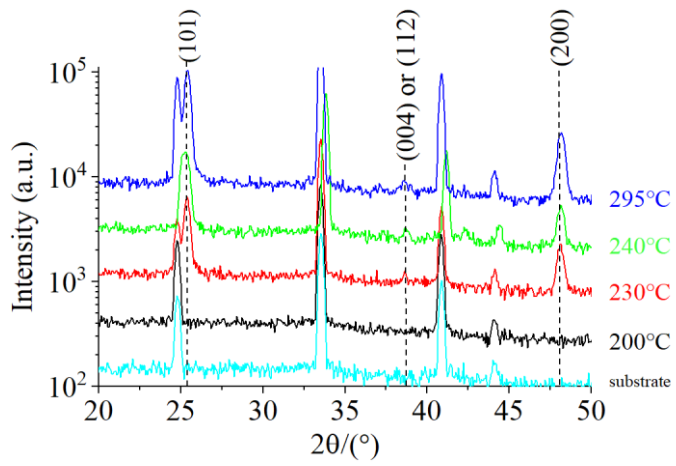


Figure 2: GIXRD patterns of TiO₂ thin films (1200 cycles) as function of selected growth temperatures. Lower graph is the bare substrate.

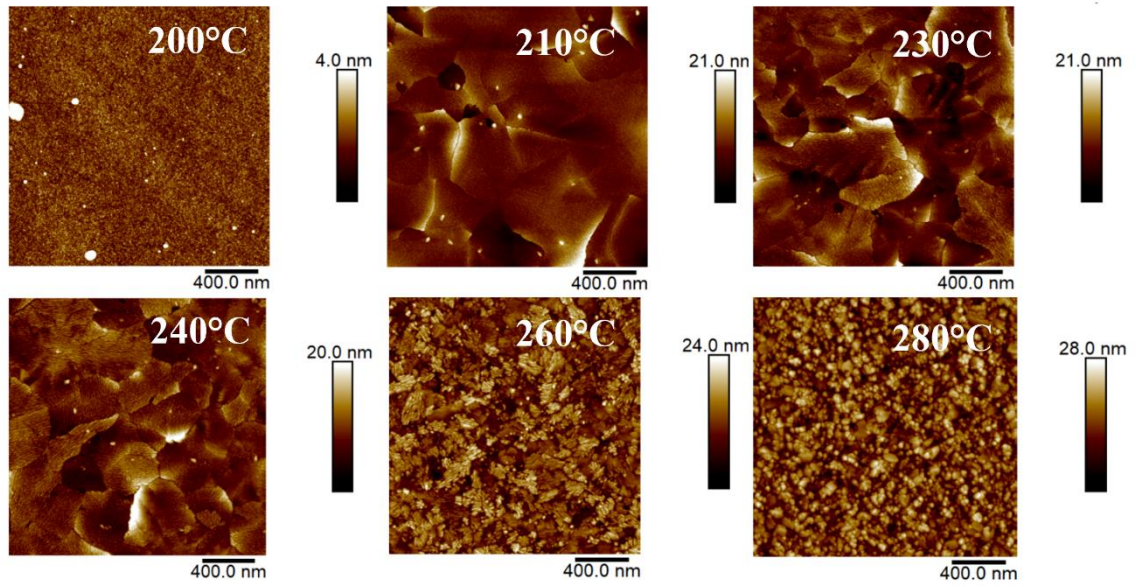


Figure 3: AFM images of 1200 cycles TiO₂ films grown at different temperatures in the range [200°C-280°C].